



Study on triphase of polymorphs TiO₂ (anatase/rutile/brookite) for boosting photocatalytic activity of metformin degradation

Diana Rakhmawaty Eddy^{a,*}, Geometry Amal Nur Sheha^a, Muhamad Diki Permana^{a,b,c}, Norio Saito^c, Takahiro Takei^c, Nobuhiro Kumada^c, Irkham^a, Iman Rahayu^a, Ikki Abe^d, Yuta Sekine^d, Tomoki Oyumi^d, Yasuo Izumi^d

^a Department of Chemistry, Faculty Mathematics and Natural Sciences, Universitas Padjadjaran, Sumedang, 45363, Indonesia

^b Special Educational Program for Green Energy Conversion Science and Technology, Integrated Graduate School of Medicine, Engineering, and Agricultural Sciences, University of Yamanashi, Kofu, 400-8511, Japan

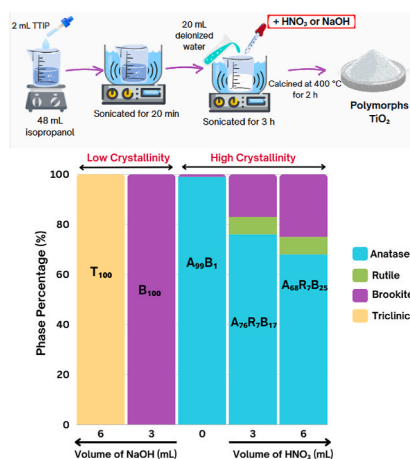
^c Center for Crystal Science and Technology, University of Yamanashi, Kofu, 400-8511, Japan

^d Department of Chemistry, Graduate School of Science, Chiba University, Chiba, 263-8522, Japan

HIGHLIGHTS

- The triphasic polymorph TiO₂ was successfully prepared by ultrasound assisted sol-gel method.
- The ratio of anatase-rutile-brookite is tuned by changing the volume of acid and base condition.
- Triphasic TiO₂ has a highest photocatalytic activity than single and biphasic phase.
- The increased photoactivity of triphasic TiO₂ is attributed to the heterojunction effect.

GRAPHICAL ABSTRACT



ARTICLE INFO

Handling editor: E. Brillas

Keywords:

Heterophase polymorph
Heterojunction
Metformin degradation
Photocatalysis
Titanium dioxide

ABSTRACT

The elution of pharmaceutical products such as metformin at higher concentrations than the safe level in aquatic systems is a serious threat to human health and the ecosystem. Photocatalytic technology using TiO₂ semiconductors potentially fixes this problem. This study aims to synthesize triphasic anatase–rutile–brookite TiO₂ using ultrasound assisted sol–gel technique in the presence of acid and its application to photodegradation of metformin under UV light irradiation. Based on X-ray diffraction analysis, a TiO₂ sample consisted of anatase (76%), rutile (7%), and brookite (17%) polymorph (A₇₆R₇B₁₇) that was fully crystallized. Scanning electron microscopy (EM)–energy dispersive X-ray spectra results showed agglomerated triphasic A₇₆R₇B₁₇ with irregular

* Corresponding author.

E-mail address: diana.rahmawati@unpad.ac.id (D.R. Eddy).

<https://doi.org/10.1016/j.chemosphere.2024.141206>

Received 13 October 2023; Received in revised form 10 January 2024; Accepted 12 January 2024

Available online 12 January 2024

0045-6535/© 2024 Elsevier Ltd. All rights reserved.

spherical clusters. Transmission EM results revealed that the crystal size of $A_{76}R_{7}B_{17}$ was 4–14 nm. The Brunauer–Emmett–Teller analysis showed the sample's specific surface area of $149 \text{ m}^2 \text{ g}^{-1}$. The degradation test of metformin demonstrated that the $A_{76}R_{7}B_{17}$ exhibited a 75.4% degradation efficiency after 120 min under UV light irradiation, significantly higher than using biphasic and single-phase TiO_2 photocatalysts. This difference could be attributed to the heterojunction effect of triphasic materials that effectively reduced electron–hole recombination rate as well as the combination of effective electron transfer from conduction band of brookite and anatase and the utilization of wider range of UV–visible light using rutile.

1. Introduction

The most common medicine for type 2 diabetes is metformin, which is also used as an anticancer agent as well as for a therapy for polycystic ovarian syndrome (Elizalde-Velázquez and Gómez-Oliván, 2019). Unlike the most medicines that are digested in the human body, metformin is difficult to degrade and easy to elute to the environment as unchanged through urine and feces (Bailey, 2017). Conventional wastewater treatment cannot completely eliminate metformin because of its physicochemical properties, e.g. high solubility, low octanol–water partition coefficient, low biodegradation rate, and high mobility in aqueous solutions (Parra-Marfil et al., 2023) as proven by Wilkinson et al. (2022); metformin is one of the most often found organic contaminants in 258 rivers and also identified in 104 nations worldwide. Such substances are seriously harmful to various living things and the environment because they cause the oxidative stress, mutagenesis, carcinogenesis, reproductive toxicity, medication resistance, and allergic reactions (Parra Marfil et al., 2023).

In this context, techniques to remove metformin from contaminated waters using various processes are attracting much attentions, such as photocatalysis using titanium dioxide (TiO_2) semiconductor (Quintão et al., 2016; Nezar and Laoufi, 2018; Chinnaiyan et al., 2019; Carbuloni et al., 2020; Prashanth et al., 2021). TiO_2 is widely used due to its stable physical and chemical properties, strong oxidizing capacity, high photocatalytic activity, and excellent biocompatibility compared to the other semiconductor materials such as SrTiO_3 , ZnO , WO_3 , ZrO_2 , and graphitic- C_3N_4 (Li et al., 2020).

Three distinct polymorphs of TiO_2 are anatase, rutile, and brookite (Wang et al., 2017). All three crystal structures comprise of distorted TiO_6 octahedra but connected in different ways. Anatase adopts a tetragonal form in which each octahedron has four common edges but no shared corners. A similar tetragonal structure exists in rutile, where two opposing edges of an octahedron are shared to form a linear chain in the $[0\ 0\ 1]$ direction. Furthermore, chains are additionally connected at their corners. In the orthorhombic crystal structure of brookite, octahedrons share three edges as well as three corners (Liao et al., 2012). Thermodynamically, the most stable phase is rutile, while anatase and brookite are metastable phases which transform to rutile at high temperatures (Ma et al., 2014).

However, the low quantum efficiency of TiO_2 photocatalysts caused by the rapid recombination of excited electron–hole pairs seriously limits the photocatalytic activity of the material (Chen and Mao, 2007). The presence of more than one TiO_2 polymorph is expected to exhibit a beneficial effect for improving electron–hole separation efficiency by reducing the recombination probability to enhance the photocatalytic performance (Mutuma et al., 2015). A typical example is commercial Evonik P25 containing anatase–rutile mixed phase exhibits a good photocatalytic activity than single phase TiO_2 due to electron–hole separation (Wang et al., 2015). On the other hand, the investigation of TiO_2 containing all three phases (anatase–rutile–brookite) is extremely limited. Furthermore, the combination effects of advantages of each polymorph (band energy level v.s. redox potential, light utilization range) were also discussed.

Moreover, reports on the preparation of triphasic TiO_2 are limited, but several are known using solvothermal methods (Liao et al., 2012), sol–gel methods (Mutuma et al., 2015), combination of ultrasound

assisted sol–gel technique and hydrothermal treatment (Kaplan et al., 2016), low temperature dissolution–precipitation on a porous micro-filtration membrane (Fischer et al., 2017), electrochemical anodization technique (Preethi et al., 2017), hydrothermal synthesis (Cano-Casanova et al., 2018, 2020), and hydrothermal methods using polymer (Xiong et al., 2019).

Herein, we report a simple method to synthesize anatase–rutile–brookite (triphasic phase TiO_2) via ultrasound-assisted sol–gel technique using Ti(IV) tetraisopropoxide (TTIP) as a precursor and acid or base as a phase control reagent. This method has been chosen because inexpensive equipment used, high homogeneity, and high purity due to the acoustic cavitation (formation, expansion, and explosion of bubbles) leading to the formation of materials with higher crystallinity (Jameel et al., 2020; Eddy et al., 2023a). To the best of our knowledge, there have been no studies using ultrasound assisted sol–gel technique to synthesize triphasic TiO_2 . The unique triphasic TiO_2 was applied for the first time to the metformin degradation under the UV light irradiation.

2. Methods

2.1. Materials

The chemicals used for the synthesis were TTIP (97%, Sigma–Aldrich, USA), isopropyl alcohol (IPA, 99%, Sigma–Aldrich), anatase and rutile (TiO_2 , 99%, Kanto Chemical Co., Japan), nitric acid (HNO_3 , 65%, Merck, USA), sodium hydroxide (NaOH , 98%, Merck), ethanol ($\text{C}_2\text{H}_5\text{OH}$, 100%, Merck), metformin-HCl ($\text{C}_4\text{H}_{11}\text{N}_5\text{HCl}$, Hexpharm Jaya, Indonesia), ammonium oxalate monohydrate ($(\text{NH}_4)_2\text{C}_2\text{O}_4\cdot\text{H}_2\text{O}$, 99%, Sigma–Aldrich), and silver nitrate (AgNO_3 , 99% Sigma–Aldrich). All chemicals were used without further purification.

2.2. Synthesis of heterophase TiO_2

Heterophase TiO_2 was prepared using ultrasound assisted sol–gel technique methods by varying the added volume of acid and/or base based on the previous reports (Quintero et al., 2020; Luthfiah et al., 2021). The acidic conditions were provided by the addition of 1 M HNO_3 (A3 and A6), while the basic conditions used 1 M NaOH (B3 and B6). Table S1 shows the various synthesis conditions of TiO_2 samples. In a typical procedure, 2 mL of TTIP was slowly added into 48 mL of IPA under vigorous, constant stirring. The solution was ultrasonicated for 20 min and 20 mL of deionized water was added. Then, acid or base solution was added dropwise to the suspension. The mixture was continuously ultrasonicated for 3 h to complete the reaction. The obtained solid was collected by centrifugation, washed with ethanol and distilled water three times, followed by drying at 343 K for 90 min. The resulting product was obtained, and calcined at 673 K for 2 h.

2.3. Characterizations

The crystal structure, phase composition, and crystallite size were analyzed by powder X-ray diffraction (XRD, Rigaku/MiniFlex 600, Tokyo, Japan) at 295 K using $\text{Cu K}\alpha$ emission (wavelength $\lambda = 0.15418 \text{ nm}$) and scans were performed in the range of $20\text{--}70^\circ$ ($2\theta_{\text{Bragg}}$) with the scan speed of $10^\circ \text{ min}^{-1}$. The resulting data were refined by the Rietveld method using a software HighScore Plus version 3.0.5 (Marvern

PANalytical, UK) to determine the crystal structure and phase composition (Permana et al., 2022). A software, Visualization for Electronic and Structural Analysis (VESTA) version 3.5.7 (Momma and Izumi, 2011) was used to visualize the crystal structure. The Debye–Scherrer Eq. (1) was used to determine the crystallite size (Patterson, 1939):

$$B = (K \lambda) / (D \cos \theta) \quad (1)$$

where B is the crystallite size (nm), K is the Scherrer constant (0.89), λ is the wavelength of X-ray (nm), D is the full width at half maximum of peak evaluated using Origin software version 8.5.1 (rad), and θ is diffraction angle (rad).

The surface morphology was characterized by scanning electron microscopy–energy dispersive X-ray spectroscopy (SEM–EDS, Tabletop Microscope-1000, Hitachi, Tokyo, Japan). Several milligrams of the sample were fixed in a sample holder. The morphology and size were examined at an acceleration voltage of 15.0 kV and magnification of 200–2000 times. Then, the EDS was measured for elemental analysis. Transmission electron microscopy (TEM; JEM-1400, JEOL Ltd, Tokyo, Japan) images were obtained at an acceleration voltage of 100 kV to examine the particle size and morphology of samples.

The specific surface area (SA) of the samples were measured based on a multipoint Brunauer–Emmett–Teller (BET) method while the pores size and pore volume were determined based on Barrett–Joyner–Halanda (BJH) method by nitrogen adsorption–desorption isotherm measurements at 77 K, using a BELSORP-mini analyzer (BEL JAPAN Inc, Tokyo, Japan).

The light absorption properties were characterized by diffuse reflectance ultraviolet–visible spectroscopy (DR UV–Vis, Jasco V-550, Tokyo, Japan) to determine the band gap (E_g) through the Davis–Mott function (Eq. (2)) (Makula et al., 2018):

$$(F(R_{\infty}) \cdot h\nu)^{1/\gamma} = B(h\nu - E_g) \quad (2)$$

in which $F(R_{\infty})$ is the Kubelka–Munk function, h is the Planck's constant, ν is the photon's frequency, B is a constant, γ is 2 for allowed indirect transition, and E_g denotes the band gap energy.

The absorption–fluorescence spectra were recorded on an FP-8600 (JASCO; Chiba Iodine Resource Innovation Center, Chiba, Japan) equipped with a 150 W Xe arc lamp (UXL-159, Ushio, Japan) and a photomultiplier tube for excitation at 300 nm within a fluorescence range of 310–800 nm. The incident excitation light from the Xe lamp was monitored by a Si photodiode, and the monitored fluorescence light emitted from the sample was normalized based on the incident light intensity at each wavelength. The photocatalyst powder (2.0 mg) was mixed with purified water (3.0 mL) and ultrasonicated (430 W, 38 kHz) for 20 min. All spectra were recorded for the suspensions in a quartz cell at 295 K.

2.4. Photocatalytic activity of metformin degradation under the UV light

The photocatalytic activity was evaluated for photodegradation of metformin under the UV light irradiation. Photocatalytic tests were performed with a 10 mg L⁻¹ metformin solution at the pH condition of 7.0. First, reactions were performed using 1.0 g L⁻¹ catalyst. Before illumination, the suspension was stirred for 30 min in dark to attain the adsorption–desorption equilibrium. Then, the suspension was placed on top of the photoreactor and irradiated by the UVB lamp (Exo Terra, Type Reptile UVB 150, 25 W) at the distance of 5 cm, under continuous stirring for 120 min. The reaction temperature was controlled using a blower so that the reactants remained at 295 K. To determine the metformin concentration during reaction tests, 3 mL solution were taken every 30 min, filtered using a 0.22- μ m polycarbonate filter membrane, and then the absorbance of the metformin solution was measured at $\lambda_{\max} = 233$ nm using a UV–vis spectrophotometer (Shimadzu, 1800; Tokyo, Japan).

The concentration of metformin was determined based on the cali-

bration following the Lambert–Beer's law. The photodegradation rate was calculated using the 1st-order Langmuir–Hinshelwood kinetic model (Eq. (3)).

$$-\ln(C_t / C_0) = kt \quad (3)$$

Where C_0 dan C_t are the concentrations before and after irradiation at a certain time, t represents the time, and k is the photodegradation rate constant. The degradation efficiency (%) was determined by Eq. (4). This photocatalytic activity test was also carried out with irradiation and the absence of catalyst (photolysis).

$$\text{Degradation efficiency (\%)} = (1 - (C_t / C_0)) \times 100 \quad (4)$$

For the optimization of reaction parameters, the catalyst dosage (0.5, 1.0, and 1.5 g L⁻¹), pH value (3, 5, 7, 9, and 11), and initial concentration of metformin (10, 15, and 20 mg L⁻¹) were varied using the best catalyst materials based on the first experiments. Furthermore, to investigate the photocatalytic mechanism, experiments of active species trapping were carried out by adding 100 mM of IPA (a quencher of \bullet OH), ammonium oxalate (OA, a quencher of h^+), AgNO₃ (a quencher of e^-), and bubbling N₂ (99.9%, 20 mL min⁻¹, remove dissolved oxygen). The detailed experimental conditions were similar to those for the other photocatalytic experiments.

3. Results and discussion

3.1. Structural Analysis

The crystallographic structures of the samples characterized by powder XRD patterns are depicted in Fig. 1a. The characteristic peak of anatase commercial appears at 25.4° (0 1 1), 37.1° (0 1 3), 37.9° (0 0 4), 38.7° (1 1 2), 48.2° (0 2 0), 54.1° (0 1 5), 55.2° (1 2 1), and 62.9° (0 2 4) diffractions. It can be referred to the Inorganic Crystal Structure Database (ICSD) 98-002-4276 for tetragonal anatase (Wagemaker et al., 2003). On the other hand, the diffraction peaks for rutile commercial appears at 27.4° (1 1 0), 36.1° (0 1 1), 39.1° (0 2 0), 41.2° (1 1 1), 44.0° (1 2 0), 54.3° (1 2 1), 56.5° (2 2 0), 62.7° (0 0 2), and 63.94° (1 3 0) diffractions that can be indexed from ICSD 98-016-5920 for tetragonal rutile (Tobaldi et al., 2010). The diffractogram for P25 Evonik showed the presence both of anatase and rutile phase. Meanwhile, the peak pattern for sample A3 with the addition of acid was consisted of major peaks owing to anatase, small peaks of rutile, and overlapping peaks of brookite. Brookite phase in sample A3 appeared at 25.4° (0 2 1), 48.1° (1 3 2), and 55.4° (1 4 2) diffractions that can be indexed from ICSD 98-007-7693 for orthorhombic brookite (Meagher and Lager, 1979).

To investigate the effect of acid and/or base addition during synthesis on the crystal phase composition, all diffractograms of the TiO₂ samples at different conditions are summarized in Fig. S1. At neutral condition, anatase was a dominant phase with a minor brookite. Furthermore, in acidic condition (A3 and A6) shows three phases (anatase, rutile, and brookite). Then, the excess amount of acid in sample A6 increased the ratio of brookite and decreased anatase phase. On the other hand, the addition of base (3 mL; Fig. S2a) resulted in peaks that can be indexed to brookite phase as the $2\theta_{\text{Bragg}}$ angles at 25.4° (0 2 1), 30.8° (1 2 1), and 48.0° (1 3 2) diffractions. Meanwhile, further addition of base (6 mL; Fig. S2b) led to triclinic or anorthic TiO₂ crystal system corresponding to peaks appeared at 31.5° (2 $\bar{2}$ 2). The details can be seen in references ICSD 98-003-5364 (Le Page and Strobel, 1982). It has been confirmed that the addition of HNO₃ and NaOH for synthesis played a critical role in tailoring the composition of anatase–rutile–brookite mixed phase TiO₂ samples. The phase ratio in the XRD data was summarized in Table 1.

Fig. 2 schematically shows the formation process of heterophase of TiO₂ polymorphs. In this research, we found that the acid or base conditions during synthesis played an important role in polymorph composition. The formation of TiO₂ under neutral and acidic conditions

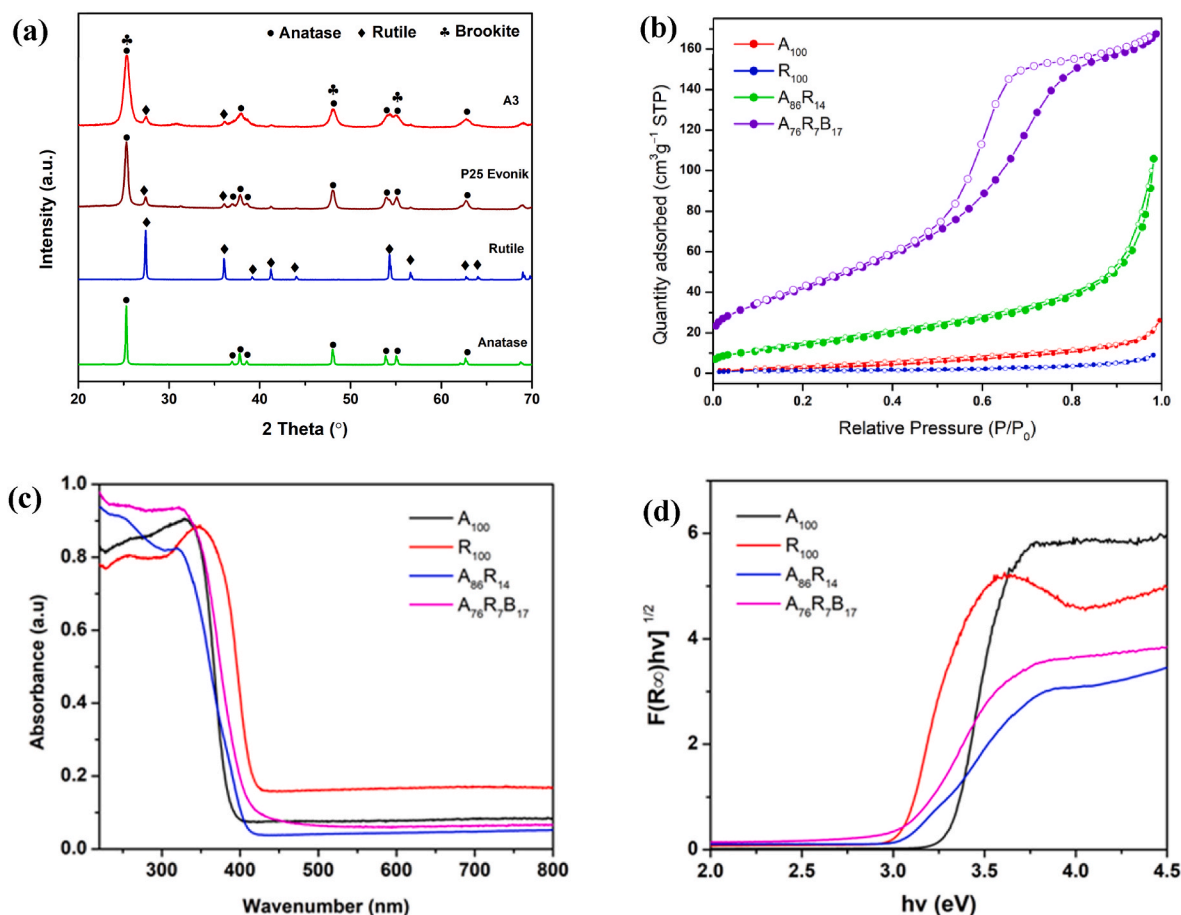


Fig. 1. XRD pattern, (b) N₂ adsorption–desorption isotherms, (c) UV–vis absorption spectra, and (d) band-gap plot using Davis–Mott equation of the samples.

Table 1
Phase ratio percentage of the samples used in this study.

Sample	Phase ratio (%) ^a				Sample Code
	Anatase	Rutile	Brookite	Triclinic TiO ₂ (Anorthic)	
Anatase	100.0 ± 0.3	–	–	–	A ₁₀₀
Rutile	–	100.0 ± 0.3	–	–	R ₁₀₀
P25 Evonik	85.8 ± 0.4	14.2 ± 0.3	–	–	A ₈₆ R ₁₄
A6	67.5 ± 0.3	7.1 ± 0.1	25.4 ± 0.5	–	A ₆₈ R ₇ B ₂₅
A3	76.0 ± 0.3	7.0 ± 0.1	17.1 ± 0.4	–	A ₇₆ R ₇ B ₁₇
N	99.2 ± 0.3	–	0.8 ± 0.1	–	A ₉₉ B ₁
B3	–	–	100.0 ± 1.1	–	B ₁₀₀
B6	–	–	–	100.0 ± 1.6	T ₁₀₀

^a Standard deviation values are also noted.

led to a high crystallinity which is later helpful for good electron transfer in view of photocatalysis. In alkaline conditions, TiO₂ led to lower crystallinity even after calcination at 673 K for 2 h. Despite the poor crystallinity under alkaline conditions, brookite peaks for B3 sample can still be identified (Pauling and Sturdivant, 1928). Under more alkaline conditions (B6), some TiO₂ was identified in the triclinic (anorthic) and orthorhombic forms. Under these conditions, TiO₂ cannot form a tetragonal structure as in anatase and rutile but undergoes distortion to form an anorthic and orthorhombic TiO₂ (Katyal et al., 1999).

Furthermore, the alkaline condition that used NaOH led to a plausible formation of sodium titanate before forming brookite by releasing Na⁺ from the surface accompanied by oxidation of Ti in the structure, and due to the incomplete transformation, sodium titanate was still detected based on the EDS (Figs. S10 and S11). This result was consistent with previous report by Tay et al. (2013).

Table S4 and Fig. S7 present the crystallite size of the samples estimated using Scherer's equation. The crystal size of synthesized mixed phase of TiO₂ was smaller than those of single-phase reference commercial anatase and rutile. In acidic media, especially for higher content of HNO₃, the crystallite size was significantly reduced. It might be concluded that crystal growth was inhibited when three phases are formed simultaneously during synthesis. Meanwhile, in neutral conditions, the crystallite size was the smallest for anatase TiO₂. On the contrary, in alkaline conditions it produced the smallest crystallite size of brookite and for higher content of NaOH led to amorphous structure.

3.2. Morphological analysis

The morphologies of single phase, biphasic, and triphasic phase were observed by SEM. Fig. 3a and b shows that A₁₀₀ and R₁₀₀ have a homogeneous smaller particle shape. Furthermore, for biphasic samples (A₈₆R₁₄) in Fig. 3c consist of smaller aggregated particles. Meanwhile, triphasic phase samples (A₇₆R₇B₁₇) depicted in Fig. 3d shows the formation of irregular clusters composed of bulk primary particles. Furthermore, EDS mappings (Fig. S8) confirmed the high purity of A₇₆R₇B₁₇ sample, containing only titanium and oxygen atoms. Then, the EDS confirmed the atomic ratio of titanium and oxygen in A₇₆R₇B₁₇ sample (Table S5). The atomic ratio of the EDS results demonstrated oxygen vacancy sites in A₇₆R₇B₁₇ sample and the empirical formula was

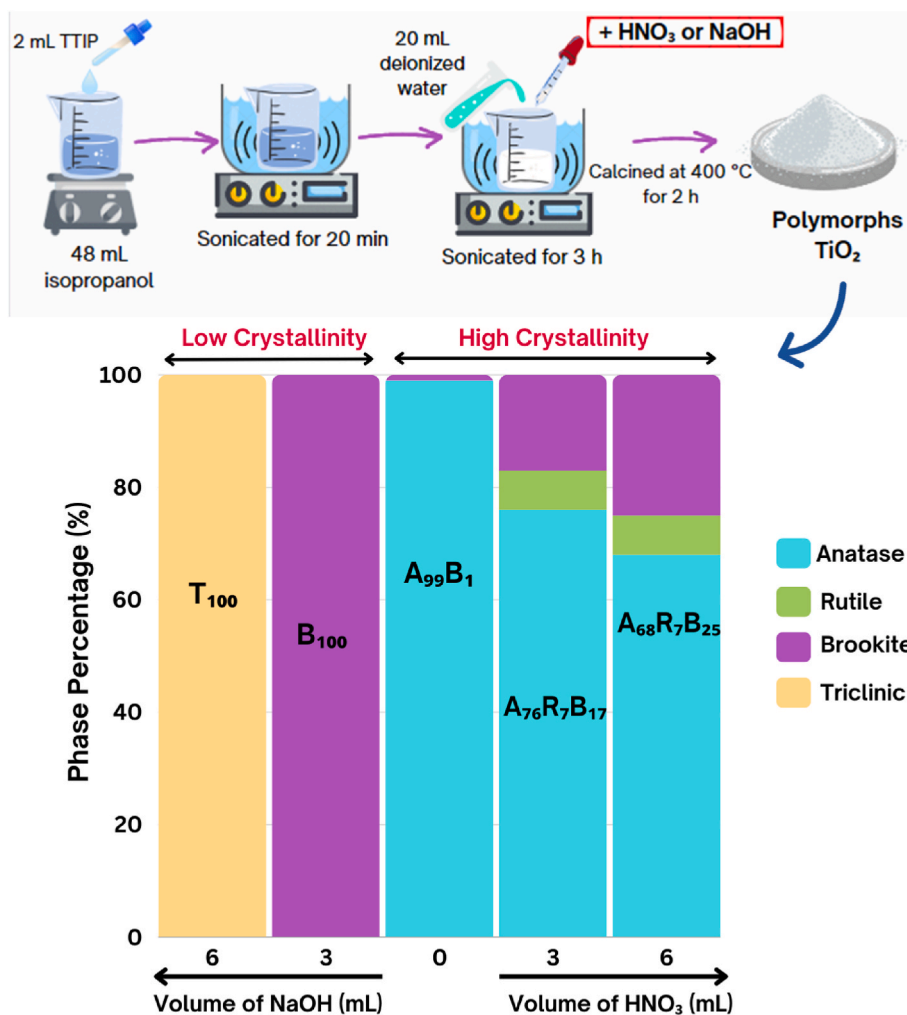


Fig. 2. Schematic representation of the formation process of TiO_2 polymorphs and the effect of acid and base volumes to control the crystal and phase compositions.

evaluated to $\text{TiO}_{1.98}$. These oxygen vacancies facilitate the charge separation at the semiconductor interface, significantly reducing the recombination of electrons and hole, thus greatly enhancing the photocatalytic activity (Chen et al., 2018).

Further characterization was performed by using TEM (Fig. 3e) to observe a closer look of $\text{A}_{76}\text{R}_7\text{B}_{17}$ that showed the presence of spherical structures. The size distribution of $\text{A}_{76}\text{R}_7\text{B}_{17}$ was shown in Fig. S9. It is known that the crystal size ranges between 4 and 14 nm. This is essentially in accordance with the calculation of the crystallite size from the XRD pattern: anatase sizes of 7–9 nm, 11–16 nm rutile, and 6–9 nm brookite for $\text{A}_{76}\text{R}_7\text{B}_{17}$ sample.

3.3. Surface analysis

Comparison of the specific SA for various TiO_2 samples is important because the morphology will affect the photocatalytic activity. Fig. 1b represents the BET plots of the TiO_2 samples. The specific SA, BJH pore radius, and BJH pore volume were evaluated (Table 2). Based on the graph, it has been observed that all samples show a type of IV isotherm according to the international union of pure and applied chemistry (IUPAC) classification. The type IV reveals that the samples have mesoporous structure (IUPAC et al., 1985). The triphasic phase ($\text{A}_{76}\text{R}_7\text{B}_{17}$) sample exhibited a larger specific SA $149.04 \text{ m}^2 \text{ g}^{-1}$ than biphasic phase ($49.9 \text{ m}^2 \text{ g}^{-1}$) and single-phase samples (9.33 and $5.13 \text{ m}^2 \text{ g}^{-1}$). The detailed results of all samples were summarized in Table S8. Photocatalyst materials with greater amount of pore volume, porosity, and

specific SA should enhance the possibility interaction and adsorption between pollutant and catalyst (Amano et al., 2010).

3.4. Optical properties

The optical properties of the samples were investigated by diffuse reflectance UV–vis spectroscopy. Fig. 1c shows the absorption spectrum of single phase, biphasic, and triphasic TiO_2 samples observed in the range of 220–800 nm. Davis–Mott plot was obtained (Fig. 1d) to determine bandgap energy value (E_g) based on Eq. (2). The absorption spectrum and bandgap value of all variant TiO_2 phases are shown in Figs. S12–S14.

The obtained E_g values for anatase (3.3 eV) are greater than rutile phase (3.1 eV), in accord with reported E_g values of TiO_2 polymorphs (Luttrell et al., 2014). On the other hand, pure brookite was reported to show a greater band gap than single phase anatase and rutile (Reyes–Coronado et al., 2008; Zhang et al., 2014). It should be noted that the values in Table 2 are slightly greater than generally reported values (3.2 for anatase, 3.0 for rutile and 3.3 eV for brookite). Meanwhile, band gap value for $\text{A}_{86}\text{R}_{14}$ have a similar value to that in our previous report (Eddy et al., 2021) while have a smaller band gap than single phase anatase. Furthermore, triphasic phase with a higher ratio of brookite phase have a E_g value of 3.1 eV. The decrease in the band gap value in heterophase is caused by charge transfer between phases of TiO_2 . This band gap value strongly affects the light absorption capacity because the lower band gap broadens the absorption range (Chen et al., 2020).

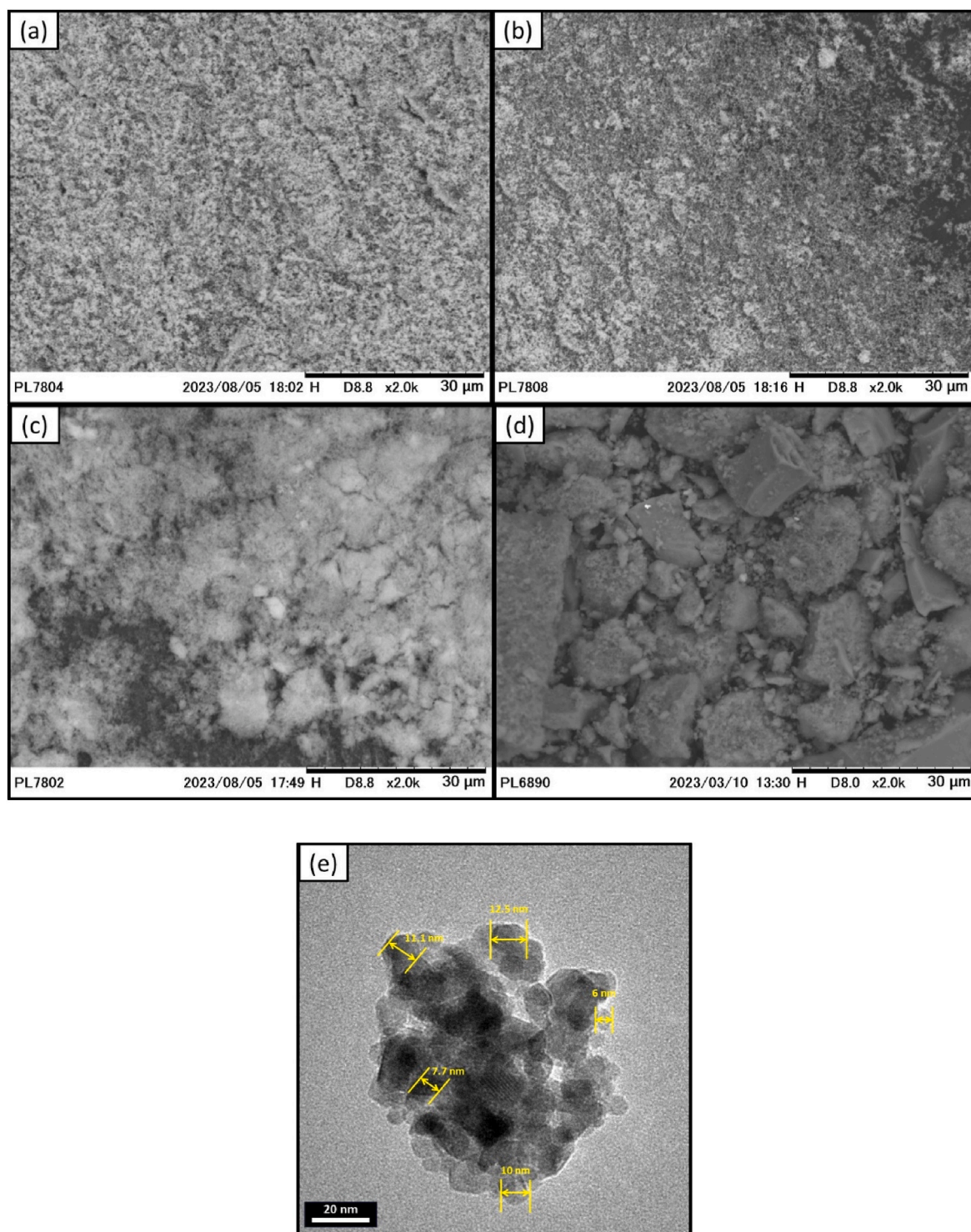


Fig. 3. SEM image of (a) A₁₀₀, (b) R₁₀₀, (c) A₈₆R₁₄, (d) A₇₆R₇B₁₇, and (e) TEM image of A₇₆R₇B₁₇.

Table 2
Band-gap value and surface properties of samples.

Samples	Band-gap Energy (eV)	Specific surface area (m ² g ⁻¹)	Pore size (nm)	Pore volume (cm ³ g ⁻¹)
A ₁₀₀	3.31	9.33	1.21	0.04
R ₁₀₀	3.05	5.13	2.71	0.01
A ₈₆ R ₁₄	3.08	49.95	1.21	0.16
A ₇₆ R ₇ B ₁₇	3.07	149.04	2.38	0.28

The mixed phase TiO₂ potentially transfers photogenerated charges between different TiO₂ polymorphs that have different band energy levels, leading to charge carriers' separations and suppressing electron-hole recombination. However, the fluorescence spectra (Fig. S15) on the time scale of 50 ms were similar for anatase, rutile, biphasic (A₈₆R₁₄), and triphasic (A₇₆R₇B₁₇). In a closer look, the energy positions of major fluorescence peak reflected direct band-gap de-excitation: 370 nm for brookite, 395 nm for anatase, and 415 nm for rutile. Due to the major peak energy shift as well as the difference of reflection/diffraction of excitation light ($\lambda = 300$ nm) to draw increasing background toward

300 nm, the fluorescence from $A_{76}R_7B_{17}$ sample looked more intense, but the intensity of effective fluorescence (the band gap de-excitation major peak and peaks related to interband impurity level at 450 and 465 nm) was similar for $A_{76}R_7B_{17}$, $A_{86}R_{14}$, and rutile. The fluorescence intensity for anatase was weaker by $\sim 30\%$ compared to the others. This fact suggested that charge separation owing to UV irradiation and oxidation/reduction reactions by the charges proceeded faster than 50 ms. As a result, the multiple-phase materials showed higher photocatalytic activity than single phase TiO_2 (Khedr et al., 2021).

As an alternative interpretation, based on the VB and CB energy

levels for these crystalline phases (see the last part of 3.5 Photocatalytic Activity section), charges are not necessarily separated via heterophase junction but rather tend to be collected at rutile VB (h^+) and CB (e^-) (Fig. 1c). Therefore, the charge separation effects at the heterophase junction were marginal, and the energy level of CB minimum above the reduction potential of $O_2/\cdot O_2^-$ (-0.046 eV @NHE) for brookite and anatase was the most critical. Secondly, oxidation ability was in the order brookite > anatase > rutile based on the energy level of VB maximum. The brookite (and anatase) should comprise key reactive species for both reduction and oxidation reactions, and combined rutile

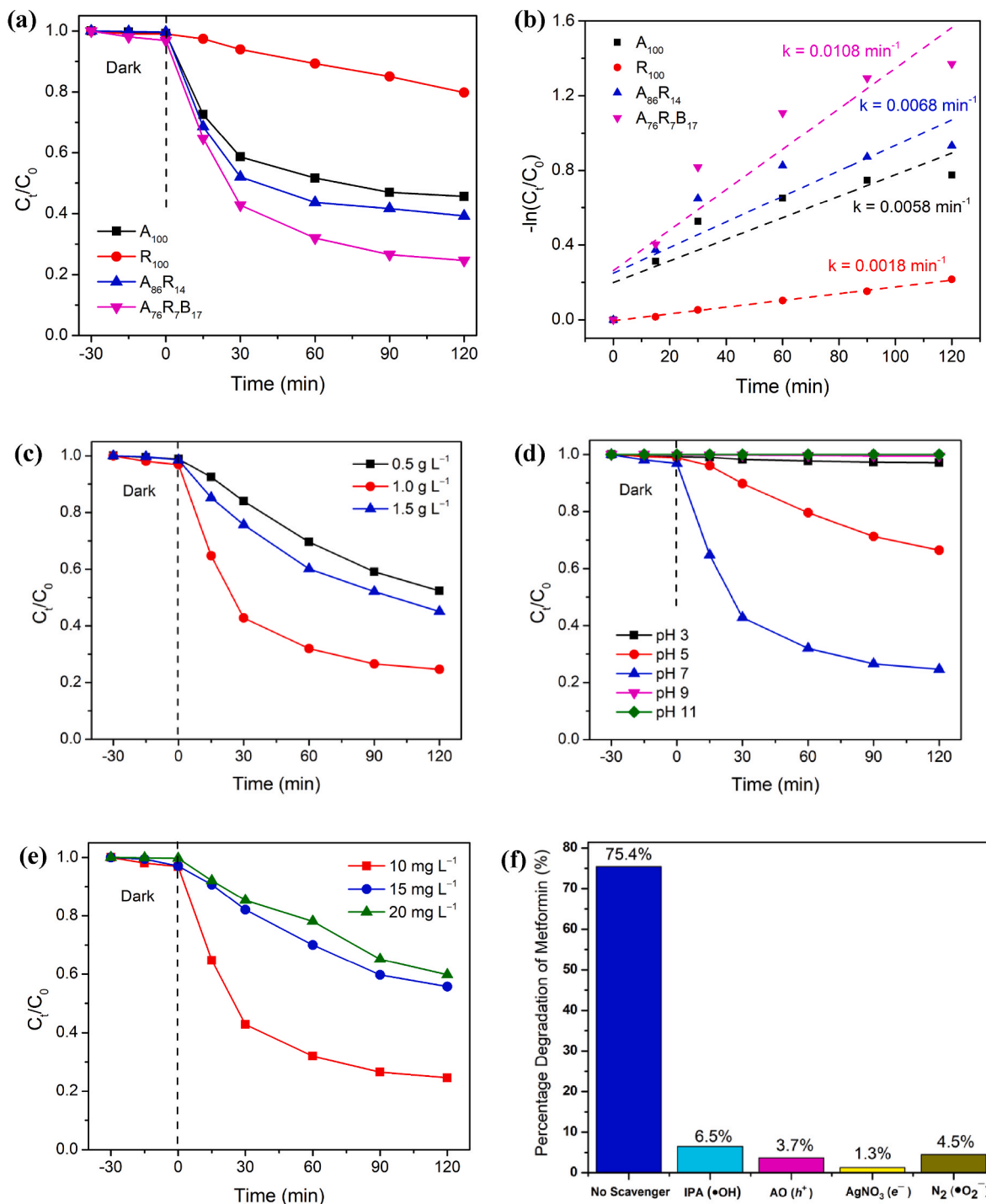


Fig. 4. (a) Photocatalytic activity, (b) reaction rate (volume = 60 mL, [metformin] = 10 mg L^{-1} , catalyst dose = 1 g L^{-1} , pH = 7), (c) photocatalytic activity of $A_{76}R_7B_{17}$ with effect of pH condition ([metformin] = 10 mg L^{-1} , catalyst dose = 1 g L^{-1}), (d) catalyst dose ([metformin] = 10 mg L^{-1} , pH = 7), (e) metformin concentration (catalyst dose = 1 g L^{-1} , pH = 7), and (f) effects of trapping agent for metformin photodegradation.

(and anatase) worked to widen the photon absorption range between 370 and 415 nm (Fig. 1c and S15) for charge separation in photocatalyst.

3.5. Photocatalytic activity

The photocatalytic properties of the various TiO₂ samples were evaluated by the photodegradation reaction of metformin under 25-W UVB lamp irradiation. Prior to the test, the direct photolysis, e.g. in the absence of photocatalyst, was investigated. As shown in Fig. S16a, no activity was observed for the photolysis for metformin degradation. When we start the UV-visible light irradiation, triphasic phase A₇₆R₇B₁₇ TiO₂ exhibited the higher activity than that using biphasic A₈₆R₁₄ and single phase of anatase (A₁₀₀) and rutile (R₁₀₀) as illustrated in Fig. 4a. It is believed that the presence of more than one polymorph suppresses the recombination of electron-hole (e⁻-h⁺) pairs, since photo-excited electrons can migrate from one phase to the other, and thus leading to an enhancement on the photocatalytic performance (Zhou et al., 2017). However, not all the heterophase have a good photocatalytic activity because it depends on the phase composition and mostly on the conduction band (CB) minimum and valence band (VB) minimum levels (Liu et al., 2019; Chalastara et al., 2020; Eddy et al., 2023b). In this study, it can be concluded that a large proportion of anatase significantly affected the photocatalytic activity. The reason why indirect band-gap anatase exhibits a longer lifetime of photoexcited electrons and holes than direct band gap of rutile and brookite is that the direct transitions of photogenerated electrons from CB to VB of anatase TiO₂ is impossible (Zhang et al., 2014). Furthermore, triphasic phase A₇₆R₇B₁₇ has the higher specific SA than single phase and biphasic phase (Table 2).

The kinetic analysis (ln C_t/C₀ versus the irradiation time) is shown in Fig. 4b and for all samples in Fig. S16b. Triphasic A₇₆R₇B₁₇ showed the greatest rate constant ($k = 0.0108 \text{ min}^{-1}$), which was 1.6, 1.9, and 6.0 times greater than biphasic A₈₆R₁₄ ($k = 0.0068 \text{ min}^{-1}$), single phase anatase A₁₀₀ ($k = 0.0058 \text{ min}^{-1}$), and single-phase rutile R₁₀₀ ($k = 0.0018 \text{ min}^{-1}$), respectively. The degradation efficiency of A₁₀₀, R₁₀₀, A₈₆R₁₄, and A₇₆R₇B₁₇ are 54.3, 20.2, 60.7, and 75.4%, respectively. The data for all samples are summarized in Table S9.

In order to verify that the major effect of photocatalytic activity is phase composition rather than the specific SA, we further designed the photocatalytic activity tests using high specific SA of anatase with 270 m² g⁻¹ (Sakai Chemical Industry Co. Ltd.) and rutile with 100 m² g⁻¹ (Sakai Chemical Industry Co. Ltd.) comparing with biphasic phase A₈₆R₁₄ with SSA 49.95 m² g⁻¹ and triphasic phase A₇₆R₇B₁₇ with SSA 149.04 m² g⁻¹. The results in Fig. S17 showed that triphasic phase A₇₆R₇B₁₇ has the highest photocatalytic activity than pure materials with high specific SA. It is confirmed that in this experiment phase composition has the main effect of photocatalytic activity. Meanwhile, high specific surface area of triphasic phase also enhance the adsorption of metformin that will improve photocatalytic activity.

Analyzing the optimization parameters, e.g. pH, catalyst concentration, substrate concentration and the presence of oxidants will affect photocatalytic activity (Reza et al., 2017). In this study, we investigated the effects of catalyst concentration, pH, and initial metformin concentration. The results in Fig. 4c showed that optimal dose for the metformin photodegradation test is 1.0 g L⁻¹ because it performs better than 0.5 g L⁻¹ and 1.5 g L⁻¹ of catalyst concentration. This is due to the decrease of active site number to interact with metformin in 0.5 g L⁻¹ of catalyst concentration (Mezener and Hamadi, 2012). Meanwhile, 1.5 g L⁻¹ was too high concentration that raised the metformin solution turbidity and light scattering, which prevented effective photon reaching the catalyst surface and thus further decreasing the degradation rate (Sun et al., 2008; Wang et al., 2023), in consistent with report by Carbuloni et al. (2020).

Then, the evaluation at different pH is shown in Fig. 4d. It was found that at lower initial pH of 3 and 5 the degradation efficiency of metformin was 2.9 and 33.6%, respectively. Further, as the pH increases, degradation efficiency of metformin increases until the initial pH of 7.0

with value 75.6%. Meanwhile, increasing the initial pH metformin until 11 conversely inactivated the photocatalyst. This could be explained by the properties of both the metformin and triphasic TiO₂. The point of zero charge (pH_{PZC}) for the photocatalyst TiO₂ is 6.25 (Chinnaiyan et al., 2019). Therefore, its surface is predominately positively charged below pH_{PZC} (i.e. TiO₂ + H⁺ ↔ TiOH₂⁺) and negatively charged above pH_{PZC} (i.e., TiOH + OH⁻ ↔ TiO⁻ + H₂O) (Mezener and Hamadi, 2012). Furthermore, a pK_a of 12.4 indicates metformin will exist almost entirely in the cationic form at pH values of 5–9 (Rao, 2014). In acidic pH, metformin and triphasic TiO₂ exhibit a repulsive effect as both are positive charged (pH < pH_{PZC}). Hence, the adsorption on the surface of TiO₂ might be limited. At pH 7, metformin is positive and triphasic TiO₂ is negative (pH > pH_{PZC}), thus favoring adsorption ability. Furthermore, in basic condition metformin and triphasic TiO₂ exhibit a repulsive effect as both are negative charged (pH > pH_{PZC}) that caused inactive adsorption ability. Thus, the trend of pH value dependence was in accord with the other reports (Chinnaiyan et al., 2019).

The effects of initial metformin concentration was also evaluated with 1.0 g L⁻¹ catalyst concentration at pH 7. Fig. 4e shows that the condition of 10 g L⁻¹ was the most favorable than the other concentrations. When the initial metformin concentration exceeded 15–20 mg L⁻¹, the degradation rate decreased. This was due to the effect of active site catalyst are covered by metformin molecules to prevent UV light reaching the catalyst surface, resulting in less radical generated that significantly reducing photocatalytic activity (Wang et al., 2023). Therefore, the optimized condition for degradation metformin using triphasic phase A₇₆R₇B₁₇ were determined at 1.0 g L⁻¹ of catalyst dose, pH 7, and 10 mg L⁻¹ initial metformin concentration.

To validate the major active species during the photocatalytic process, experiments using a series of scavengers have been performed for A₇₆R₇B₁₇ photocatalyst. Different scavengers with 100 mM of IPA, ammonium oxalate (OA), AgNO₃, and N₂ gas (99.9%, 20 mL min⁻¹) as trapping/preventing agents for ·OH, h⁺, e⁻, and ·O₂⁻, respectively, was added to reaction system. The obtained data in Fig. 4f shows that the activity was significantly decreased in the presence of all scavengers. These results indicated that ·OH, h⁺, e⁻, and ·O₂⁻ are all the key species for metformin degradation reaction.

The plausible mechanism for the photocatalytic activity of triphasic phase A₇₆R₇B₁₇ can be evaluated theoretically by determining the positions of VB and CB using equations Eq. (5) and (6):

$$E_{VB} = \chi - E^C + 0.5 E_g \quad (5)$$

$$E_{CB} = E_{VB} - E_g \quad (6)$$

The χ represents the absolute electronegativity of semiconductors, which is defined as the geometric mean of the absolute electronegativity of the constituent atoms. χ value for TiO₂ anatase, rutile, and brookite is 5.81 eV (Usgodaarachchi et al., 2022). E^C is the energy of the free electrons on the normal hydrogen electrode scale (4.50 eV) and E_g is band gap energy of the material. The band gap of TiO₂ anatase, rutile, and brookite is 3.31, 3.05, and 3.47 eV, respectively, were obtained from DR UV-vis analyses. The parameter toward the calculation of VB and CB energy position has been tabulated in Table S10. Based on the calculated band gap energy of the VB and CB position of anatase, brookite, and rutile, a possible schematic illustration of the possible heterojunction mechanism for photocatalytic activity of triphasic phase A₇₆R₇B₁₇ was shown in Fig. 5.

When the material was exposed to UV light, the electrons were excited from VB to CB and leave holes in VB. The excited electron will migrate from brookite to anatase to rutile and the holes transfer in the same direction. This assumption is accord with reports by Kaplan et al. (2016) and Preethi et al. (2017). The accumulated electron in rutile reduced O₂ into ·O₂⁻ because VB of brookite is more negative than O₂/·O₂⁻ potential (-0.046 eV vs. NHE) (Rosman et al., 2020). Moreover, the accumulated holes in rutile capable to develop ·OH due to the VB position more positive than OH⁻/·OH potential (+2.38 eV vs. NHE)

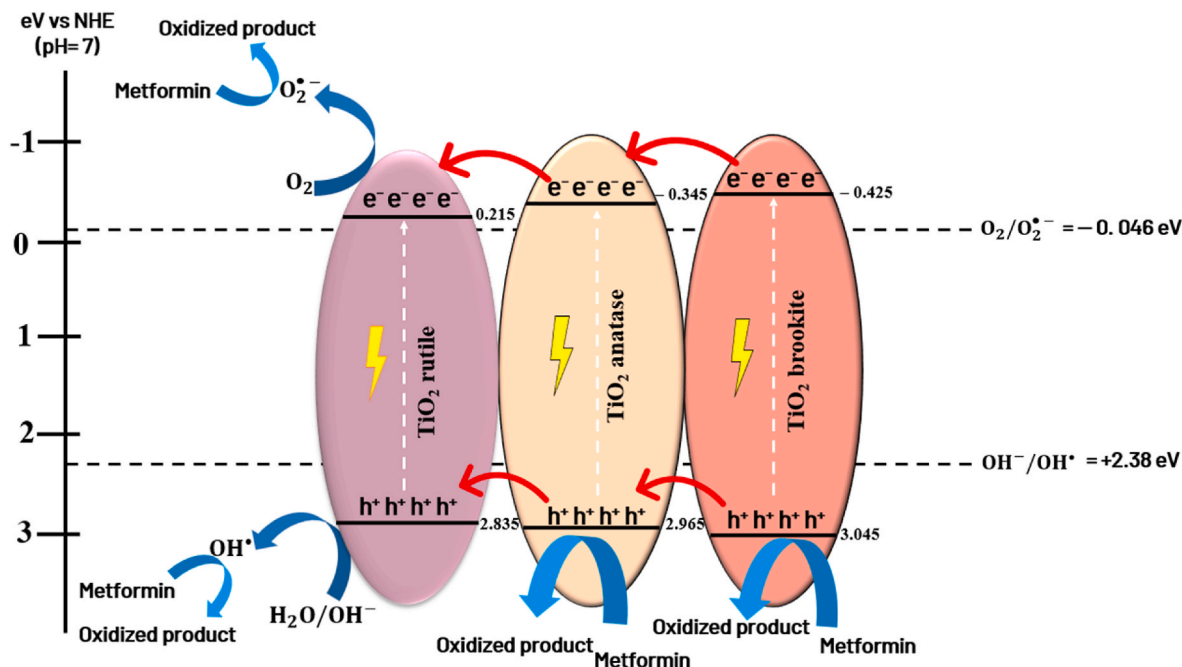


Fig. 5. Proposed mechanism of $A_{76}R_{7}B_{17}$ for metformin photodegradation.

(Rosman et al., 2020). Furthermore, based on Fig. 4f, holes also oxidized metformin directly. Both of these radical will oxidized metformin into non-toxic product such as guanyl urea ($C_2H_6N_4O$) (Quintão et al., 2016; Carbuloni et al., 2020). On the basis of the aforementioned experimental outcomes, two junction interfaces highly facilitate interfacial charge transfer compared to single junction anatase-rutile or pure phase anatase or rutile. The performance of the photocatalytic system will be improved by this interfacial charge transfer process, which enhanced the life of charge carriers.

4. Conclusions

The triphasic polymorph of TiO_2 was successfully prepared by ultrasound assisted sol-gel procedure in the presence of acid condition. The ratio of anatase-rutile-brookite is easily tuned by changing the volume of acid and base. The efficiency of triphasic TiO_2 for metformin photodegradation is compared with pure anatase, pure rutile, and biphasic TiO_2 (anatase-rutile). It is found that triphasic TiO_2 with 76% anatase, 7% rutile, and 17% brookite has a highest photocatalytic activity than single and biphasic phase. This could be the result of synergistic effects in polymorph that suppress electron-hole recombination. Furthermore, the high specific SA also give an impact but did not crucial since pure anatase and pure rutile with larger specific SA have lower photocatalytic activity.

CRediT authorship contribution statement

Diana Rakhmawaty Eddy: Conceptualization, Funding acquisition, Project administration, Supervision, Validation. **Geometry Amal Nur Sheha:** Data curation, Formal analysis, Methodology, Resources, Writing - original draft. **Muhamad Diki Permana:** Data curation, Formal analysis, Methodology, Software, Writing - original draft, Writing - review & editing. **Norio Saito:** Data curation, Formal analysis. **Takahiro Takei:** Data curation, Formal analysis. **Nobuhiro Kumada:** Data curation, Formal analysis, Supervision. **Irkham:** Data curation, Formal analysis, Software, Data curation, Formal analysis, Software. **Iman Rahayu:** Funding acquisition, Supervision. **Ikki Abe:** Data curation, Formal analysis. **Yuta Sekine:** Data curation, Formal analysis. **Tomoki Oyumi:** Data curation, Formal analysis. **Yasuo Izumi:**

Conceptualization, Data curation, Investigation, Supervision, Validation, Writing - review & editing.

Declaration of competing interest

The authors declare the following financial interests/personal relationships which may be considered as potential competing interests: Diana Rakhmawaty Eddy reports was provided by Padjadjaran University Faculty of Mathematics and Natural Sciences. Yasuo Izumi reports a relationship with Chiba University that includes: non-financial support.

Data availability

No data was used for the research described in the article.

Acknowledgements

Authors are grateful for the facilities from Universitas Padjadjaran, Indonesia, by Academic Leadership Grant (ALG), Prof. Iman Rahayu (ID: 1549/UN6.3.1/PT.00/2023), Hibah Riset Unpad (HRU) by Riset Kompetensi Dosen Unpad (RKDU), Diana Rakhmawaty Eddy (ID: 1549/UN6.3.1/PT.00/2023), and World Class Professor (WCP) Program Directorate of Resources, Directorate General of Education and Technology, Ministry of Education and Culture in 2023 grant.

Appendix A. Supplementary data

Supplementary data to this article can be found online at <https://doi.org/10.1016/j.chemosphere.2024.141206>.

References

- Amano, F., Nogami, K., Tanaka, M., Ohtani, B., 2010. Correlation between surface area and photocatalytic activity for acetaldehyde decomposition over bismuth tungstate particles with a hierarchical structure. *Langmuir* 26, 7174–7180. <https://doi.org/10.1021/la904274c>.
- Bailey, C.J., 2017. Metformin: historical overview. *Diabetologia* 60, 1566–1576. <https://doi.org/10.1007/s00125-017-4318-z>.
- Cano-Casanova, L., Amorós-Pérez, A., Ouzzine, M., Lillo-Rodenas, M.A., Román-Martínez, M.C., 2018. One step hydrothermal synthesis of TiO_2 with variable HCl

- concentration: detailed characterization and photocatalytic activity in propene oxidation. *Appl. Catal. B Environ.* 220, 645–653. <https://doi.org/10.1016/j.apcatb.2017.08.060>.
- Cano-Casanova, L., Mei, B., Mul, G., Lillo-Ródenas, M.Á., Román-Martínez, M. del C., 2020. Photocatalytic oxidation of propane using hydrothermally prepared anatase-brookite-rutile TiO₂ samples. An in situ drifts study. *Nanomaterials* 10, 1314. <https://doi.org/10.3390/nano10071314>.
- Carbuloni, C.F., Savoia, J.E., Santos, J.S.P., Pereira, C.A.A., Marques, R.G., Ribeiro, V.A.S., Ferrari, A.M., 2020. Degradation of metformin in water by TiO₂-ZrO₂ photocatalysis. *J. Environ. Manage.* 262, 110347 <https://doi.org/10.1016/j.jenvman.2020.110347>.
- Chalastara, K., Guo, F., Elouatik, S., Demopoulos, G.P., 2020. Tunable composition aqueous-synthesized mixed-phase TiO₂ nanocrystals for photo-assisted water decontamination: comparison of anatase, brookite and rutile photocatalysts. *Catalysts* 10, 407. <https://doi.org/10.3390/catal10040407>.
- Chen, P., Liu, H., Cui, W., Lee, S.C., Wang, L., Dong, F., 2020. Bi-based photocatalysts for light-driven environmental and energy applications: structural tuning, reaction mechanisms, and challenges. *EcoMat* 2, e12047. <https://doi.org/10.1002/eom2.12047>.
- Chen, S., Xiao, Y., Wang, Y., Hu, Z., Zhao, H., Xie, W., 2018. A facile approach to prepare black TiO₂ with oxygen vacancy for enhancing photocatalytic activity. *Nanomaterials* 8, 245. <https://doi.org/10.3390/nano8040245>.
- Chen, X., Mao, S.S., 2007. Titanium dioxide nanomaterials: synthesis, properties, modifications, and applications. *Chem. Rev.* 107, 2891–2959. <https://doi.org/10.1021/cr0500535>.
- Chinnaiyan, P., Thampi, S.G., Kumar, M., Balachandran, M., 2019. Photocatalytic degradation of metformin and amoxicillin in synthetic hospital wastewater: effect of classical parameters. *Int. J. Environ. Sci. Technol.* 16, 5463–5474. <https://doi.org/10.1007/s13762-018-1935-0>.
- Eddy, D.R., Ishmah, S.N., Permana, M.D., Firdaus, M.L., Rahayu, I., El-Badry, Y.A., Hussein, E.E., El-Bahy, Z.M., 2021. Photocatalytic phenol degradation by silica-modified titanium dioxide. *Appl. Sci.* 11, 9033. <https://doi.org/10.3390/app11199033>.
- Eddy, D.R., Luthfiah, A., Permana, M.D., Deawati, Y., Firdaus, M.L., Rahayu, I., Izumi, Y., 2023a. Rapid probing of self-cleaning activity on polyester coated by titania–natural silica nanocomposite using digital image-based colorimetry. *ACS Omega* 8, 7858–7867. <https://doi.org/10.1021/acsomega.2c07606>.
- Eddy, D.R., Permana, M.D., Sakti, L.K., Sheha, G.A.N., Solihudin Hidayat, S., Takei, T., Kumada, N., Rahayu, I., 2023b. Heterophase polymorph of TiO₂ (anatase, rutile, brookite, TiO₂ (B)) for efficient photocatalyst: fabrication and activity. *Nanomaterials* 13, 704. <https://doi.org/10.3390/nano13040704>.
- Elizalde-Velázquez, G., Gómez-Oliván, L., 2019. Occurrence, toxic effects and removal of metformin in the aquatic environments in the world: recent trends and perspectives. *Sci. Total Environ.* 702, 134924 <https://doi.org/10.1016/j.scitotenv.2019.134924>.
- Fischer, K., Gawel, A., Rosen, D., Krause, M., Abdul Latif, A., Griebel, J., Prager, A., Schulze, A., 2017. Low-temperature synthesis of anatase/rutile/brookite TiO₂ nanoparticles on a polymer membrane for photocatalysis. *Catalysts* 7, 209. <https://doi.org/10.3390/catal7070209>.
- Iupac, K.S., Everett, D., Haul, R., Moscou, L., Pierotti, R., Rouquerol, J., 1985. Reporting physisorption data for gas/solid systems with special reference to the determination of surface area and porosity. *Pure Appl. Chem.* 57, 603–619. <https://doi.org/10.1351/pac198557040603>.
- Jameel, M.S., Aziz, A.A., Dheyab, M.A., 2020. Comparative analysis of platinum nanoparticles synthesized using sonochemical-assisted and conventional green methods. *Nano-Struct. Nano-Objects* 23, 100484. <https://doi.org/10.1016/j.nano.2020.100484>.
- Kaplan, R., Erjavec, B., Dražić, G., Grdadolinik, J., Pintar, A., 2016. Simple synthesis of anatase/rutile/brookite TiO₂ nanocomposite with superior mineralization potential for photocatalytic degradation of water pollutants. *Appl. Catal. B Environ.* 181, 465–474. <https://doi.org/10.1016/j.apcatb.2015.08.027>.
- Katyal, N.K., Parkash, R., Ahluwalia, S.C., Samuel, G., 1999. Influence of titania on the formation of tricalcium silicate. *Cem. Concr. Res.* 29, 355–359. [https://doi.org/10.1016/S0008-8846\(98\)00231-2](https://doi.org/10.1016/S0008-8846(98)00231-2).
- Khedr, T.M., El-Sheikh, S.M., Kowalska, E., Abdeldayem, H.M., 2021. The synergistic effect of anatase and brookite for photocatalytic generation of hydrogen and diclofenac degradation. *J. Environ. Chem. Eng.* 9, 106566 <https://doi.org/10.1016/j.jece.2021.106566>.
- Le Page, Y., Strobel, P., 1982. Structural chemistry of the Magnéli phases Ti_nO_{2n-1}, 4 ≤ n ≤ 9. II. Refinements and structural discussion. *J. Solid State Chem.* 44, 273–281. [https://doi.org/10.1016/0022-4596\(82\)90374-7](https://doi.org/10.1016/0022-4596(82)90374-7).
- Li, R., Li, T., Zhou, Q., 2020. Impact of titanium dioxide (TiO₂) modification on its application to pollution treatment—a review. *Catalysts* 10, 804. <https://doi.org/10.3390/catal10070804>.
- Liao, Y., Que, W., Jia, Q., He, Y., Zhang, J., Zhong, P., 2012. Controllable synthesis of brookite/anatase/rutile TiO₂ nanocomposites and single-crystalline rutile nanorods array. *J. Mater. Chem.* 22, 7937–7944. <https://doi.org/10.1039/C2JM16628C>.
- Liu, R., Li, H., Duan, L., Shen, H., Zhang, Q., Zhao, X., 2019. Influences of annealing atmosphere on phase transition temperature, optical properties and photocatalytic activities of TiO₂ phase-junction microspheres. *J. Alloys Compd.* 789, 1015–1021. <https://doi.org/10.1016/j.jallcom.2019.02.198>.
- Luthfiah, A., Permana, M.D., Deawati, Y., Firdaus, M.L., Rahayu, I., Eddy, D.R., 2021. Photocatalysis of nanocomposite titania–natural silica as antibacterial against *Staphylococcus aureus* and *Pseudomonas aeruginosa*. *RSC Adv.* 11, 38528–38536. <https://doi.org/10.1039/D1RA07043F>.
- Luttrell, T., Halpegamage, S., Tao, J., Kramer, A., Sutter, E., Batzill, M., 2014. Why is anatase a better photocatalyst than rutile?—Model studies on epitaxial TiO₂ films. *Sci. Rep.* 4, 1–8. <https://doi.org/10.1038/srep04043>.
- Ma, Y., Wang, X., Jia, Y., Chen, X., Han, H., Li, C., 2014. Titanium dioxide-based nanomaterials for photocatalytic fuel generations. *Chem. Rev.* 114, 9987–10043. <https://doi.org/10.1021/cr500008u>.
- Makula, P., Pacia, M., Macyk, W., 2018. How to correctly determine the band gap energy of modified semiconductor photocatalysts based on UV–vis spectra. *J. Phys. Chem. Lett.* 9, 6814–6817. <https://doi.org/10.1021/acs.jpcclett.8b02892>.
- Meagher, E.P., Lager, G.A., 1979. Polyhedral thermal expansion in the TiO₂ polymorphs; refinement of the crystal structures of rutile and brookite at high temperature. *Can. Mineral.* 17, 77–85.
- Mezener, Y., Hamadi, A., 2012. Antidiabetic degradation by photocatalysis in aqueous systems on TiO₂ powders. *Res. Rev. BioSci.* 6, 378–384.
- Momma, K., Izumi, F., 2011. In: VESTA 3 for Three-Dimensional Visualization of Crystal, Volumetric and Morphology Data. *J. Appl. Cryst.* 44, pp. 1272–1276.
- Mutuma, B.K., Shao, G.N., Kim, W.D., Kim, H.T., 2015. Sol–gel synthesis of mesoporous anatase–brookite and anatase–brookite–rutile TiO₂ nanoparticles and their photocatalytic properties. *J. Colloid Interface Sci.* 442, 1–7. <https://doi.org/10.1016/j.jcis.2014.11.060>.
- Nezar, S., Laoufi, N.A., 2018. Electron acceptors effect on photocatalytic degradation of metformin under sunlight irradiation. *Sol. Energy* 164, 267–275. <https://doi.org/10.1016/j.solener.2018.02.065>.
- Parra-Marfil, A., López-Ramón, M.V., Aguilar-Aguilar, A., García-Silva, I.A., Rosales-Mendoza, S., Romero-Cano, L.A., Bailón-García, E., Ocampo-Pérez, R., 2023. An efficient removal approach for degradation of metformin from aqueous solutions with sulfate radicals. *Environ. Res.* 217, 114852 <https://doi.org/10.1016/j.envres.2022.114852>.
- Patterson, A.L., 1939. The Scherrer formula for X-ray particle size determination. *Phys. Rev.* 56, 978. <https://doi.org/10.1103/PhysRev.56.978>.
- Pauling, L., Sturdivant, J.H., 1928. XV. The crystal structure of brookite. *Z. für Kristallogr. - Cryst. Mater.* 68, 239–256. <https://doi.org/10.1524/zkri.1928.68.1.239>.
- Permana, M.D., Noviyanti, A.R., Lestari, P.R., Kumada, N., Eddy, D.R., Rahayu, I., 2022. Enhancing the photocatalytic activity of TiO₂/Na₂Ti₆O₁₃ composites by gold for the photodegradation of phenol. *ChemEngineering* 6, 69. <https://doi.org/10.3390/chemengineering6050069>.
- Prashanth, V., Priyanka, K., Remya, N., 2021. Solar photocatalytic degradation of metformin by TiO₂ synthesized using *Calotropis gigantea* leaf extract. *Water Sci. Technol.* 83, 1072–1084. <https://doi.org/10.2166/wst.2021.040>.
- Preethi, L.K., Mathews, T., Nand, M., Jha, S.N., Gopinath, C.S., Dash, S., 2017. Band alignment and charge transfer pathway in three phase anatase-rutile-brookite TiO₂ nanotubes: an efficient photocatalyst for water splitting. *Appl. Catal. B Environ.* 218, 9–19. <https://doi.org/10.1016/j.apcatb.2017.06.033>.
- Quintão, F.J.O., Freitas, J.R.L., de Fátima Machado, C., Aquino, S.F., de Queiroz Silva, S., de Cássia Franco Afonso, R.J., 2016. Characterization of metformin by-products under photolysis, photocatalysis, ozonation and chlorination by high-performance liquid chromatography coupled to high-resolution mass spectrometry. *Rapid Commun. Mass Spectrom.* 30, 2360–2368. <https://doi.org/10.1002/rcm.7724>.
- Quintero, Y., Mosquera, E., Diosa, J., García, A., 2020. Ultrasonic-assisted sol–gel synthesis of TiO₂ nanostructures: influence of synthesis parameters on morphology, crystallinity, and photocatalytic performance. *J. Sol. Gel Sci. Technol.* 94, 477–485. <https://doi.org/10.1007/s10971-020-05263-6>.
- Rao, C.V., 2014. Biguanides. In: *Encyclopedia of Toxicology*, third ed. Elsevier, Amsterdam, pp. 452–455.
- Reyes-Ronad, D., Rodríguez-Gattorno, G., Espinosa-Pesqueira, M.E., Cab, C., De Coss, R.D., Oskam, G., 2008. Phase-pure TiO₂ nanoparticles: anatase, brookite and rutile. *Nanotechnology* 19, 145605. <https://doi.org/10.1088/0957-4484/19/14/145605>.
- Reza, K.M., Kurny, A.S.W., Gulshan, F., 2017. Parameters affecting the photocatalytic degradation of dyes using TiO₂: a review. *Appl. Water Sci.* 7, 1569–1578. <https://doi.org/10.1007/s13201-015-0367-y>.
- Rosman, N., Salleh, W.N.W., Mohamed, M.A., Harun, Z., Ismail, A.F., Aziz, F., 2020. Constructing a compact heterojunction structure of Ag₂CO₃/Ag₂O in-situ intermediate phase transformation decorated on ZnO with superior photocatalytic degradation of ibuprofen. *Sep. Purif. Technol.* 251, 117391 <https://doi.org/10.1016/j.seppur.2020.117391>.
- Sun, J., Qiao, L., Sun, S., Wang, G., 2008. Photocatalytic degradation of Orange G on nitrogen-doped TiO₂ catalysts under visible light and sunlight irradiation. *J. Hazard Mater.* 155, 312–319. <https://doi.org/10.1016/j.jhazmat.2007.11.062>.
- Tay, Q., Liu, X., Tang, Y., Jiang, Z., Sum, T.C., Chen, Z., 2013. Enhanced photocatalytic hydrogen production with synergistic two-phase anatase/brookite TiO₂ nanostructures. *J. Phys. Chem. C* 117, 14973–14982. <https://doi.org/10.1021/jp4040979>.
- Tobaldi, D.M., Tucci, A., Skapin, A.S., Esposito, L., 2010. Effects of SiO₂ addition on TiO₂ crystal structure and photocatalytic activity. *J. Eur. Ceram. Soc.* 30, 2481–2490. <https://doi.org/10.1016/j.jeurceramsoc.2010.05.014>.
- Usgodaarachchi, L., Thambiliyagodage, C., Wijesekera, R., Vigneswaran, S., Kandanapitiye, M., 2022. Fabrication of TiO₂ spheres and a visible light active α-Fe₂O₃/TiO₂-rutile/TiO₂-anatase heterogeneous photocatalyst from natural ilmenite. *ACS Omega* 7, 27617–27637. <https://doi.org/10.1021/acsomega.2c03262>.
- Wagemaker, M., Kearley, G.J., Van Well, A.A., Mutka, H., Mulder, F.M., 2003. Multiple Li positions inside oxygen octahedra in lithiated TiO₂ anatase. *J. Am. Chem. Soc.* 125, 840–848. <https://doi.org/10.1021/ja028165q>.

- Wang, C., Bai, H., Kang, X., 2023. Optimization study on synergistic system of photocatalytic degradation of AR 26 and UV-LED heat dissipation. *Catalysts* 13, 669. <https://doi.org/10.3390/catal13040669>.
- Wang, H., Gao, X., Duan, G., Yang, X., Liu, X., 2015. Facile preparation of anatase–brookite–rutile mixed-phase N-doped TiO₂ with high visible-light photocatalytic activity. *J. Environ. Chem. Eng.* 3, 603–608. <https://doi.org/10.1016/j.jece.2015.02.006>.
- Wang, X., Zhao, Y., Mølhave, K., Sun, H., 2017. Engineering the surface/interface structures of titanium dioxide micro and nano architectures towards environmental and electrochemical applications. *Nanomaterials* 7, 382. <https://doi.org/10.3390/nano7110382>.
- Wilkinson, J.L., Boxall, A.B.A., Kolpin, D.W., Leung, K.M.Y., Lai, R.W.S., Galbán-Malagón, C., Adell, A.D., Mondon, J., Metian, M., Marchant, R.A., 2022. Pharmaceutical pollution of the world's rivers. *Proc. Natl. Acad. Sci. USA* 119, e2113947119. <https://doi.org/10.1073/pnas.2113947119>.
- Xiong, H., Wu, L., Liu, Y., Gao, T., Li, K., Long, Y., Zhang, R., Zhang, L., Qiao, Z., Huo, Q., 2019. Controllable synthesis of mesoporous TiO₂ polymorphs with tunable crystal structure for enhanced photocatalytic H₂ production. *Adv. Energy Mater.* 9, 1901634. <https://doi.org/10.1002/aenm.201901634>.
- Zhang, J., Zhou, P., Liu, J., Yu, J., 2014. New understanding of the difference of photocatalytic activity among anatase, rutile and brookite TiO₂. *Phys. Chem. Chem. Phys.* 16, 20382–20386. <https://doi.org/10.1039/C4CP02201G>.
- Zhou, P., Xie, Y., Liu, L., Song, J., Chen, T., Ling, Y., 2017. Bicrystalline TiO₂ heterojunction for enhanced organic photodegradation: engineering and exploring surface chemistry. *RSC Adv.* 7, 16484–16493. <https://doi.org/10.1039/C6RA28658E>.